Non-S-Wave Pairing Symmetries in Superconducting in and Sn Nanoparticles

Ma-Hsuan Ma
National Central University
Erdembayalag Batsaikhan
National Central University
Huang-Nan Chen
National Central University
Ting-Yang Chen
National Central University
Chi-Hung Lee
National Central University
Wen-Hsien Li (whli@phy.ncu.edu.tw)
National Central University
Chun-Ming Wu
National Synchrotron Radiation Research Center
Chin-Wei Wang
National Synchrotron Radiation Research Center

Research Article

Keywords: Superconductivity, Ferromagnetism, Nanoparticles, Magnetization, Magnetic proximity, Neutron diffraction

Posted Date: August 2nd, 2021

DOI: https://doi.org/10.21203/rs.3.rs-735305/v1

Abstract

We report on experimental evidence of non-*s*-wave pairing in In and Sn nanoparticle assemblies. Spontaneous magnetizations are observed, through extremely weak-field magnetization and neutron-diffraction measurements, to develop when the nanoparticles enter the superconducting state. The superconducting transition temperature T_C shifts to a noticeably higher temperature when an external magnetic field or magnetic Ni nanoparticles are introduced into the vicinity of the superconducting In or Sn nanoparticles. There is a critical magnetic field and a critical Ni composition that must be reached before the magnetic environment will suppress the superconductivity. Development of spin-parallel superconducting pairs on the surfaces and spin-antiparallel superconducting pairs in the core of the nanoparticles is used to understand the observations.

Introduction

Phonon-mediated *s*-wave pairing between the electrons near the Fermi level forms spin-singlet (S = 0) Cooper pairs. This pairing has become the backbone of BCS superconductivity. The BSC mechanism explains most, if not all, of the physical properties associated with the so-called conventional weak-coupling superconductor. In this context, the elements In and Sn, in their bulk form, behave as a standard BCS-type superconductor, where the magnetic environment will destroy the spin-singlet pairings. In principle, Cooper pairs can also form in other symmetries, such as the spin-triplet *p*-wave[1,2], or can be mediated through other quasi-particles, such as spin fluctuations[3-5]. Spin-triplet *p*-wave superconductivity has been identified in the heavy-fermion compound UPt_3[(6,7)] as well as in the quasi-two-dimensional ruthenate Sr_2RuO_4[(8,9)]. Spin-singlet *d*-wave pairing has been found in the high-T_C cuprate $YBa_2Cu_3O_7$[(10)]. Cooper-pair moments can develop in the superconducting state that is associated with a spin-triplet pairing, as has been observed in Sr_2RuO_4 by polarized neutron diffraction studies[11,12]. Although the superconductivity of elements in their bulk form is believed to be associated with the spin-singlet *s*-wave pairing, it is now known that superconducting parameters depend strongly on the physical size of the system[13-24]. Although the most noticeable finite size effect is the loss of superconductivity upon reaching the Anderson criterion[25-27] when the electron level separation near the Fermi level becomes comparable to the BCS superconducting gap. There is, however, a particular range in particle size which reveals nonconventional superconductivity prior to entering the Anderson regime. Our previous results reveal noticeable enhancement of the superconducting transition temperature T_C and critical magnetic field H_C in extremely space-restricted Pb[(15,16)], In[(18)], Sn[(23)] and Al[(24)] nanoparticles before reaching the Anderson regime. Furthermore, the superconductivity which coexists with ferromagnetism at low temperatures[23,24] can be attributed to the enhanced superconductivity that survives from the local spin polarized ferromagnetic moments developed in the nanoparticles.

In searching for superconductivity in quantum sized nanoparticles from other than BCS pairings, we study the effects of an external magnetic field or magnetic proximity on the superconductivity in extremely space-restricted In and Sn nanoparticles. Here, we report on the results of magnetization,

magnetic susceptibility, resistivity and neutron diffraction measurements made on In, Sn and In/Ni nanoparticle assemblies. Development of additional magnetization in the superconducting state is revealed. The existence of an intrinsic magnetic moment in the superconducting state is confirmed by the neutron diffraction measurements. An enhancement of superconductivity by the application of an external magnetic field was observed, with the enhancement in T_C becoming even larger with the introduction of magnetic Ni nanoparticles into the nanoparticle assembly. An inverse magnetic proximity effect was also observed. T_C of the superconducting nanoparticles increases noticeably, when magnetic Ni nanoparticles are introduced into the vicinity of the superconducting nanoparticles. These effects are then reversed when the external magnetic field reaches a critical strength or when the concentration of the neighboring magnetic Ni nanoparticles reaches a critical composition. These results indicate the appearance of non-*s*-wave coupling for the superconductivity of In and Sn nanoparticles.

Materials And Methods

Synthesis of nanoparticles. Two sets of In (designated as In-A and In-B), one of Sn (designated as Sn-A), and one of Ni (designated as Ni-A) nanoparticles were fabricated employing the gas-condensation method, following the steps taken in Ref. 15. High-purity (99.99%) In/Sn/Ni spheres (2-2.5 mm in diameter) were evaporated in an Ar atmosphere at selective pressures (Table 1), using an evaporation rate of 0.05 Å/s. The evaporated particles were collected on a non-magnetic plate, which was placed 20 cm above the evaporation source and the temperature was maintained at 77 K. After restoration to room temperature, the nanoparticles, which were only loosely attached to the collector, were stripped off from the collector plate. The samples thus obtained were in powdered form and consisted of a macroscopic amount of individual In/Sn/Ni nanoparticles. There were no substrates or capping molecules on these nanoparticles. The nanoparticles were kept in a vacuum at all times, expect when being mixed together before being loading into the sample holders. This was done in an Ar atmosphere and took less than 5 minutes.

Methods. The nanoparticle (NP) assembly was obtained by thoroughly mixing nanoparticles A and B with a mass ratio of A : B = m : n, hereafter designated as $(A)_m(B)_n$. For example, $(In\text{-}A)_{90}(Ni\text{-}A)_{10}$ indicates that in this sample, the mass ration of In-A : Ni-A = 90 : 10. After mixing, the powder was shaken at 10 Hz for 3 minutes using a Vortex-Genie Mixer. Packing fraction of $f \equiv \frac{\text{mass density of the nanoparticle assembly}}{\text{mass density of its counterpart in bulk form}} \times 100\%$ is used to specify the mean separation between nanoparticles in the assembly.

The x-ray diffraction measurements were conducted using a Bruker D8 ADVANCE diffractometer with an incident wavelength of l = 1.5406 Å from a copper target, a Bruker LynxEye linear position sensitive detector (PSD) captured a scattering angle of 4^o, and a Ni filter was placed before the PSD to screen the K_β radiation. The diffraction patterns were taken in the reflection geometry. The neutron diffraction measurements were conducted at the Bragg Institute, ANSTO, using the high intensity powder diffractometer Wombat, employing Ge(113) monochromator crystals to select an incident wavelength

of l = 2.412 Å and a cylindrical vanadium-can to hold the nanoparticles (~0.7 g). The sample temperature was controlled using a He-gas closed-cycle refrigeration system.

Magnetization, ac magnetic susceptibility, dc electrical resistivity and specific heat measurements were all performed on a Physical Property Measurement System manufactured by Quantum Design, employing the standard setup. For the magnetization and susceptibility measurements, the nanoparticles (~70 mg) were packed into a non-magnetic cylindrical holder also from Quantum Design, which produces a smooth temperature curve and background signals which are ~4% that of the sample. For the resistivity measurements, samples in the form of solid pieces were obtained by cold-pressing the powder flat using a mechanical pressure of 5-20 kgW/cm^2 (depending on the designed packing fraction), after thoroughly mixing nanoparticles in the designed mass ratios. The typical sample size was ~2×2×0.1 mm^3 which could be handled normally. The resistivity data were collected using the standard four-probe setup, operated in constant current mode. The specific-heat data were collected employing the thermal relaxation method, with a charcoal pump placed near the sample platform to avoid He condensation. The nanoparticles were supported using the N-Grease by Apiezon, which produces ~5% of the total signal and a smooth temperature curve.

Sample characterization. Figure 1a show the x-ray diffraction pattern of the representative Sn-A NP assembly, revealing the NPs crystallize into the same structure as their bulk counterpart. There are no identifiable traces of oxidation phases in the diffraction patterns. As expected, the diffraction peaks appear to be much broader than the instrumental resolution, reflecting the broadening of the peak profiles from the finite-size effect. The mean particle diameter and size distribution of the NP assembly were determined by fitting the diffraction peaks to the diffraction profiles of finite sized particles[28]. The solid curves in Fig. 1a indicate the diffraction pattern calculated assuming a log-normal size distribution (inset to Fig. 1a) with a mean particle diameter of 10.0(3) nm and a standard deviation of 0.21(2) for the Sn-A NP assembly. The chamber pressure used during evaporation, the mean particle diameter and the standard deviation of size distribution for the four sets of NP assemblies are listed in Table 1.

Results And Discussion

Ferromagnetic spin polarization. The isothermal magnetization curves M(H_a) of the NP assemblies reveal a rapid increase with increasing H_a in the low H_a regime, reaching saturation at a higher H_a. Figure 1b shows representative M(H_a) curves of 7 nm In-A (open triangles) and 7 nm Sn-A (solid circles) NP assemblies taken at 300 K. The M(H_a) can be described (solid curves on data) very well by a Langevin profile of $M(H_a) = M_S[\coth(x)-(1/x)]$, where M_S is the saturation magnetization, $x \equiv \mu_P H_a/k_B T$, μ_p is the mean particle moment and k_B is the Boltzmann's constant, giving M_S = 0.126(2) and 0.279(2) emu/g for the In-A and Sn-A NP assemblies, respectively, at 300 K. The Langevin behavior of M(H_a) may be understood as the alignment of a randomly oriented assembly of magnetic nanoparticles, each characterized by a superspin with a mean particle moment μ_p, at a temperature T by the applied magnetic field H_a. Similar Langevin M(H_a) curves were also observed for the 4.5 nm Ni-A NP assembly, giving a M_S

= 28.0(2) emu/g at 300 K. Note that the M_S of bulk Ni is 58.6 emu/g at 300 K. The M_S for the four sets of NP at 300 K are listed in Table 1. A larger M_S was obtained for a smaller In NPs (Table 1). This reveals that the contribution from the surface spins to particle superspin dominates that from the core spins in In NPs. On the other hand, a smaller M_S was obtained for Ni NPs, showing the core spins dominate over the surface spins in Ni NPs.

Ferromagnetic Moment in Superconducting State. A packing fraction of $f \approx 5\%$ is frequently obtained when naturally packs the assembly into a holder. Using the holder shown in the inset to Fig. 2b, the packing fraction can easily be adjusted by turning the tap cap. This set-up allows us to fine tune the packing fraction of the assembly and to perform measurements on the very same nanoparticles at different packing fractions. The highest achievable packing fraction obtained in the present study is f = 75%. Figure 2 displays the temperature dependence of the magnetization M and the in-phase component c¢ of the ac magnetic susceptibility, taken at various packing fractions, of the In-B (Fig. 2a) and Sn-A (Fig. 2b) NP assemblies. The magnetizations were measured without the presence of an external magnetic field or a driving magnetic field, except a residual dc magnetic field of ~3 Oe that may still appear, but to detect the magnetization induced in the sensing coil when the sample was removed from the coil. This measures the spontaneous magnetic moment of the sample. The c¢, on the other hand, measures the response when the sample is subjected to a weak probing ac magnetic field. This reveals the response of the sample to the probing magnetic field. The diamagnetic c¢ signals the appearance of superconductivity at low temperatures. These c¢(T) can be described (solid curves) by Scalapino's expression[29] to give T_C = 3.486(3) and 3.714(2) K for In-B at f = 53% and Sn-A at f = 36%, respectively.

Interestingly, spontaneous magnetizations appear in the superconducting regime. The magnetization begins to develop at a temperature that is slightly but noticeably lower than the development of superconductivity. This component disappears in the normal state. It appears that superconductivity triggers the development of spontaneous magnetization, with the magnetic moment points, in some degree, in the same direction of macroscopic magnetization of the assembly. This is a behavior that will not appear in the superconducting state with a spin-single S = 0 pairing, but favors a spin-triplet S = 1 pairing that can coexist with ferromagnetism[30]. The M(T) curves measured with an applied magnetic field H_a exhibit a diamagnetic screening effect, as expected.

The existence of intrinsic magnetic moments in 7 nm Sn-A and 10.6 nm In-B NP assemblies is confirmed by the neutron diffraction measurements. Increases in the reflection intensities of the 7 nm Sn NPs upon cooling from 4 to 2.8 K are clearly revealed in the difference pattern between the diffraction patterns taken at 2.8 and 4 K (Fig. 3a). These magnetic intensities appear at the positions of the nuclear Bragg reflections, showing the development of a ferromagnetic moment upon cooling from 4 to 2.8 K. The width of the magnetic peak is the same as that of the associated nuclear Bragg reflection, showing that the magnetic moments are distributed throughout the whole nanoparticle, rather than being located solely on the surface. Unfortunately, the difference between the magnetic moments of the ions in the core and on the surface cannot be resolved, if they are indeed different, at the instrumental resolution used in the

present study. Order parameter measurement reveals the integrated intensity of the (200)+(101) reflections increases progressive with decreasing temperature, with a sharp change in the increase rate below 4 K (Fig. 3b). In the normal state the (200)+(101) intensity increases by ~19% upon cooling from 200 to 4 K, and an additional 10% increase is seen upon entering the superconducting state on further cooling from 4 to 1.65 K. The thermal reduction rates of the magnetic intensities in the normal and superconducting states differ by a factor of 42, showing that they are associated with different origins. The magnetic diffraction pattern shown in Fig. 3a can be described (solid curve) reasonably well by assuming the development of a ferromagnetic moment of $<m_Z> = 0.064\ m_B$ that points in the [101] crystallographic direction. The moment developed in the superconducting state upon cooling from 4 to 1.65 K is $<m_Z> = 0.046\ m_B$. A similar behavior of sharp increases in the (110) intensity upon entering the superconducting state is also seen in the 10.6 nm In-A NP assembly (Fig. 3c), revealing the development of an additional ferromagnetic moment in the superconducting state for the 10.6 nm In NPs.

Superconductivity Enhanced by an External Magnetic Field. The zero-field thermal specific heat of the In-B NP assembly departs greatly from the normal state behavior of $\gamma T+\beta T^3$ upon cooling to below 3.5 K, reflecting the appearance of superconductivity below $T_C = 3.5$ K (Fig. 4a), which is 3% higher than the $T_C = 3.41$ K of bulk In. A lattice coefficient of $\beta = 2.32$ mJ/mole-K^2, corresponding to a Debye temperature of 113 K, is obtained for the 10.6 nm In NPs, showing a reduction of 12% in the Debye temperature upon reduction of the particle diameter to 10.6 nm. Two components, marked Δ_1 and Δ_2, that respond differently to H_a are seen in the electronic specific heat obtained by subtracting the βT^3 contribution from the data (Fig. 4b). Clearly, Δ_1 is associated with the occurrence of superconductivity. The application of an H_a greatly enhances the electronic specific heat in the superconducting transition regime below as well as above T_C, with the enhancement becoming smaller at a higher H_a. The creation of a spin-polarized gap near the Fermi level by the H_a cannot account for the observed characteristic H_a-dependence of Δ_1, since a larger H_a will generate a larger spin-polarized gap. It clearly shows that the application of an H_a will alter the electronic behavior in the superconducting state. The Δ_2 that appears at 2.2 K is less sensitive to the H_a. It is linked to the emergence of the discrete electron level, known as the Kubo gap, near the Fermi level in the 10.6 nm In NPs. A Kubo gap of 0.18 meV is expected for the 10.6 nm In NPs, when is estimated according to the Kubo formula[31-33]. This energy gap, which corresponds to a thermal energy of 2.1 K, agrees with the thermal position of Δ_2.

The enhancement of T_C by the application of a magnetic field H_a is seen in the $(In\text{-}A)_{100-x}(Ni\text{-}A)_x$ NP assemblies. T_C of $(In\text{-}A)_{95}(Ni\text{-}A)_5$ increases progressively as H_a increases from 0 to 250 Oe (Fig. 5a), but then decreases with a further increase in H_a (Fig. 5b). In addition, the diamagnetic response, represented by the value of c¢ at 2 K $c¢_{2K}$, is stronger as H_a increases from 0 to 250 K, but becomes weaker upon a further increase in H_a (open triangles in Fig. 5c). The c¢(T) can be described by Scalapino's expression (solid curves in Figs. 5a and 5b) used to extract T_C together with the density of states (DOS) near the Fermi level D_F[29]. T_C of the 7 nm In NPs increases from 2.89 K at $H_a = 0$ to 3.21 K at $H_a = 250$ Oe. The 11%

increase of T_C by an H_a of 250 Oe is accompanied by a 40% increase of D_F (Fig. 5d). T_C, D_F and $c¢_{2K}$ reach their maxima at H_a = 250 Oe, above which these superconducting parameters are gradually suppressed by the increase of H_a. Apparently, it is the increase of the DOS near the Fermi level by the application of a magnetic field that strengthen the superconductivity in the 7 nm In NPs. The enhancement of T_C by an H_a is also seen in the $(In\text{-}A)_{90}(Ni\text{-}A)_{10}$ NP assembly, but T_C is suppressed by an H_a in the 15% Ni-A NP assembly of $(In\text{-}A)_{85}(Ni\text{-}A)_{15}$ (Fig. 6). Clearly, there are two competing factors at work, one enhancing while the other suppresses the superconductivity which affect the superconductivity in the 7 nm In NPs under an applied magnetic field.

Conclusion

The superconductivity that operates in the present In and Sn nanoparticles is different in nature from that which operates in bulk In and Sn. The inverse magnetic proximity effect observed in quench-condensed Pb/Ag films[34] that originated from the leakage of conduction electrons from the Ag to the neighboring Pb films will not appear in the present In/Ni NP assemblies, since the conduction electron density of Ni nanoparticles is significantly lower than that of In nanoparticles. It is very unlikely that an external magnetic field as weak as 300 Oe can cause a 5% softening in phonon frequencies to account for the 17% increase in T_C. A pairing mechanism that can be enhanced by the magnetic field is indeed needed to understand the present observations of T_C can be enhanced by an external magnetic field or by magnetic neighbors. The spin-triplet *p*-wave pairing which has been observed in Sr_2RuO_4 and UPt_3 could be a candidate. The observation that superconductivity is eventually suppressed once the external magnetic field or the neighboring magnetic content exceeds a critical composition, showing that there is a superconducting component that can be suppressed by magnetic proximity. The quantum confinement is not yet significant in the present nanoparticles, showing that the surface atoms play a key role. One possible configuration for the superconducting pairing is that the antiparallel spin pairings develop mainly at the core, while the parallel spin pairings appear mainly on the surface. In this configuration, an external magnetic field would help with the formation of parallel spin pairings on the surface, but suppress antiparallel spin pairings in the core. Below the critical magnetic field the effect from the surface dominates to enhance superconductivity. Above this point, the magnetic field suppresses superconductivity when the effect from the core dominated.

Declarations

Acknowledgements

This work was supported by the Ministry of Science and Technology of Taiwan under Grant No. MOST 110-2112-M-008-034. We acknowledge the Ministry of Science and Technology, Taiwan for financial support through Grant No. MOST-108-2739-M-213-001 from National Synchrotron Radiation Research Center (NSRRC) Neutron Cultivation Program, in providing the neutron scattering facility used in this work.

Author Contributions

W.H.L., C.H.L. designed the study; M.H.M., E.B., T.Y.C., C.M.W., C.W.W., W.H.L. performed the measurements; M.H.M., E.B., T.Y.C. C.H.L. analyze the data; all of the authors discussed the results; W.H.L., M.H.M. wrote the manuscript.

Additional Information

Competing Interests: The authors declare no competing interests.

References

1. Mackenzie, A. P. & Maeno, Y. The superconductivity of Sr_2RuO_4 and the physics of spin-triplet pairing. *Rev. Mod. Phys*. **75**, 657-712 (2003). https://doi.org/10.1103/RevModPhys.75.657
2. Wang, W.-S., Zhang, C.-C., Zhang, F.-C. & Wang, Q.-H. Theory of Chiral p-Wave Superconductivity with Near Nodes for Sr_2RuO_4. *Phys. Rev. Lett*. **122**, 027002 (2019). https://doi.org/10.1103/PhysRevLett.122.027002
3. Bednorz, J. G. & Muller, K. A. *Earlier and Recent Aspects of Superconductivity*, 1st ed. P 315 (Springer-Verlag: Berlin Heidelberg, Germany, 1990).
4. Duan, C., Sasmal, K., Maple, M. B., Podlesnyak, A., Zhu, J.-X., Si, Q. & Dai, P. Incommensurate Spin Fluctuations in the Spin-Triplet Superconductor Candidate UTe_2. *Phys. Rev. Lett*. **125**, 237003 (2020). https://doi.org/10.1103/PhysRevLett.125.237003
5. Jenni, K., Kunkemöller, S., Steffens, P., Sidis, Y., Bewley, R., Mao, Z. Q., Maeno, Y. & Braden, M. Neutron scattering studies on spin fluctuations in Sr_2RuO_4. *Phys. Rev. B* **103**, 104511 (2021). https://doi.org/10.1103/PhysRevB.103.104511
6. Tou, H., Kitaoka, Y., Asayama, K., Kimura, N., Ōnuki, Y., Yamamoto, E. & Maezawa, K. Odd-Parity Superconductivity with Parallel Spin Pairing in UPt_3: Evidence from ^{195}Pt Knight Shift Study. *Phys. Rev. Lett*. **77**, 1374-1377 (1996). https://doi.org/10.1103/PhysRevLett.77.1374
7. Joynt, R. & Taillefer, L. The superconducting phases of UPt_3. *Rev. Mod. Phys*. **74**, 235-294 (2002). https://doi.org/10.1103/RevModPhys.74.235
8. Mackenzie, A. P. & Maeno, Y. The superconductivity of Sr_2RuO_4 and the physics of spin-triplet pairing. *Rev. Mod. Phys*. **75**, 657-712 (2003). https://doi.org/10.1103/RevModPhys.75.657
9. Maeno, Y., Kittaka, S., Nomura, T., Yonezawa, S. & Ishida, K. Evaluation of Spin-Triplet Superconductivity in Sr_2RuO_4. *J. Phys. Soc. Jpn*. **81**, 011009 (2012). https://doi.org/10.1143/JPSJ.81.011009
10. Tsuei, C. C. & Kirtley, J. R. Pairing symmetry in cuprate superconductors. *Rev. Mod. Phys*. **72**, 969-1016 (2000). https://doi.org/10.1103/RevModPhys.72.969
11. Duffy, J. A., Hayden, S. M., Maeno, Y., Mao, Z., Kulda, J. & McIntyre, G. J. Polarized-Neutron Scattering Study of the Cooper-Pair Moment in Sr_2RuO_4. *Phys. Rev. Lett*. **85**, 5412-5415 (2000).

https://doi.org/10.1103/PhysRevLett.85.5412

12. Steffens, P., Sidis, Y., Kulda, J., Mao, Z. Q., Maeno, Y., Mazin, I. I. & Braden, M. Spin Fluctuations in Sr_2RuO_4 from Polarized Neutron Scattering: Implications for Superconductivity. *Phys. Rev. Lett.* **122**, 047004 (2019). https://doi.org/10.1103/PhysRevLett.122.047004
13. Bezryadin, A. & Lau, C., Tinkham, M. Quantum suppression of superconductivity in ultrathin nanowires. *Nature* **404**, 971–974 (2000). https://doi.org/10.1038/35010060
14. Reich, S., Leitus, G., Popovitz-Biro, R. & Schechter, M. Magnetization of Small Lead Particles. *Phys. Rev. Lett.* **91**, 147001 (2003). https://doi.org/10.1103/PhysRevLett.91.147001
15. Wu, C.-M., Karna, S. K., Liu, S.-B. Inverse magnetic proximity effects in superconducting In-Ni and Sn-Ni nanoparticle assemblies. *J. Nanopart. Res.* **15**, 1691 (2013). https://doi 10.1007/s11051-013-1691-5
16. Li, W.-H., Yang, C. C., Tsao, F. C. & Lee, K. C. Quantum size effects on the superconducting parameters of zero-dimensional Pb nanoparticles. *Phys. Rev. B* **68**, 184507 (2003). https://doi.org/10.1103/PhysRevB.68.184507
17. Bose, S., Raychaudhuri, P., Banerjee, R., Vasa, P. & Ayyub, P. Mechanism of the Size Dependence of the Superconducting Transition of Nanostructured Nb. *Phys. Rev. Lett.* **95**, 147003 (2005). https://doi.org/10.1103/PhysRevLett.95.147003
18. Li, W.-H., Yang, C. C., Tsao, F. C., Wu, S.Y., Huang, P. J., Chung, M. K. & Yao, Y. D. Enhancement of superconductivity by the small size effect in In nanoparticles. *Phys. Rev. B* **72**, 214516 (2005). https://doi.org/10.1103/PhysRevB.72.214516
19. Guo, Y., Zhang, Y. F., Bao, X.-Y., Han, T.-Z., Tang, Z., Zhang, L.-X., Zhu, W.-G., Wang, E.G., Niu, Q., Qiu, Z.Q., Jia, J.-F., Zhao, Z.-X. & Xue, Q.-K. Superconductivity Modulated by Quantum Size Effects. *Science* **306**, 1915-1917 (2004). https://doi.org/10.1126/science.1105130
20. Moshchalkov, V. V., Gielen, L., Strunk, C., Jonckheere, R. & Qiu, X., Van Haesendonck, C., Bruynseraede, Y. Effect of sample topology on the critical fields of mesoscopic superconductors. *Nature* **373**, 319-322 (1995). https://doi.org/10.1038/373319a0
21. LeClair, P., Moodera, J. S., Philip, J. & Heiman, D. Coexistence of Ferromagnetism and Superconductivity in Ni/Bi Bilayers. *Phys. Rev. Lett.* **94**, 037006 (2005). https://doi.org/10.1103/PhysRevLett.94.037006
22. Bose, S., Garcia-Garcia, A. M., Ugeda, M. M., Urbina, J. D., Michaelis, C. H., Brihuega, I. & Kern, K. Observation of shell effects in superconducting nanoparticles of Sn. *Nature Mater* **9**, 550–554 (2010). https://doi.org/10.1038/nmat2768
23. Li, W.-H., Wang, C.-W., Li, C.-Y., Hsu, C. K., Yang, C. C. & Wu, C.-M. Coexistence of ferromagnetism and superconductivity in Sn nanoparticles. *Phys. Rev. B* **77**, 094508 (2008). https://doi.org/10.1103/PhysRevB.77.094508
24. Liu, S.-B., Chen, C.-T., Wu, C.-M., Wang, C.-W., Wang, C.-J., Karna, S. K. & Li, W.-H. Suppression of superconductivity by interparticle interactions in Al nanoparticle assembly. *J. Appl. Phys.* **109**, 07E153 (2011). https://doi.org/10.1063/1.3564936

25. Anderson, P. W. Theory of dirty superconductors. *J. Phys. Chem. Solids* **11**, 26-30 (1959). https://doi.org/10.1016/0022-3697(59)90036-8
26. von Delft, J., Zaikin, A. D., Golubev, D. S. & Tichy, W. Parity-Affected Superconductivity in Ultrasmall Metallic Grains. *Phys. Rev. Lett*. **77**, 3189-3192 (1996). https://doi.org/10.1103/PhysRevLett.77.3189
27. Smith, R. A. & Ambegaokar, V. Effect of Level Statistics on Superconductivity in Ultrasmall Metallic Grains. *Phys. Rev. Lett*. **77**, 4962-4965 (1996). https://doi.org/10.1103/PhysRevLett.77.4962
28. Li, W.-H. & Lee, C.-H. Spin polarization and small size effect in bare silver nanoparticles. In *Complex Magnetic Nanostructures Synthesis, Assembly and Applications*, 1st ed.; Sharma, S., Eds. p 195–224, (Springer International Publishing: New York, NY, USA, 2017).
29. Mühlschlegel, B., Scalapino, D. J. & Dento, R. Thermodynamic Properties of Small Superconducting Particles. *Phys. Rev. B* **6**, 1767-1777 (1972). https://doi.org/10.1103/PhysRevB.6.1767
30. Keizer, R. S., Goennenwein, S. T .B., Klapwijk, T.M., Miao, G., Xiao, G. & Gupta, A. A spin triplet supercurrent through the half-metallic ferromagnet CrO_2. *Nature* **439**, 825-827 (2006). https://doi.org/10.1038/nature04499.
31. Halperin, W. P. Quantum size effects in metal particles. *Rev. Mod. Phys*. **58**, 533-606 (1986). https://doi.org/10.1103/RevModPhys.58.533
32. Kubo, R. Electronic properties of metallic fine particles. I. *J. Phys. Soc. Jpn*. **17**, 975–986 (1962). https://doi.org/10.1143/JPSJ.17.975
33. Kawabata, A. & Kubo, R. Electronic properties of fine metallic particles. II. Plasma resonance absorption. *J. Phys. Soc. Jpn*. **21**, 1765–1772 (1962). https://doi.org/10.1143/JPSJ.21.1765
34. Bourgeois, O., Frydman, A. & Dynes, R. C. Inverse Proximity Effect in a Strongly Correlated Electron System. *Phys. Rev. Lett*. **88**, 186403 (2002). https://doi.org/10.1103/PhysRevLett.88.186403

Tables

Table 1: Chamber pressures used during evaporation, mean particle diameters, standard deviation widths of the size distributions, saturation magnetizations at 300 K, and labels used for the nanoparticle assemblies used in this study.

Element	P (torr)	<d> (nm)	σ	M_S (emu/g)	Label
In	2.0	7.0(2)	0.11(1)	0.126(4)	In-A
In	1.0	10.6(4)	0.12(1)	0.105(5)	In-B
Sn	1.5	7.0(4)	0.18(4)	0.279(3)	Sn-A
Ni	4.5	4.5(3)	0.11(2)	28.0(2)	Ni-A

P = Chamber pressure used during evaporation

<d> = Mean particle diameter

σ = Standard deviation width of size distribution

M_S = Saturation magnetization at 300 K

Figures

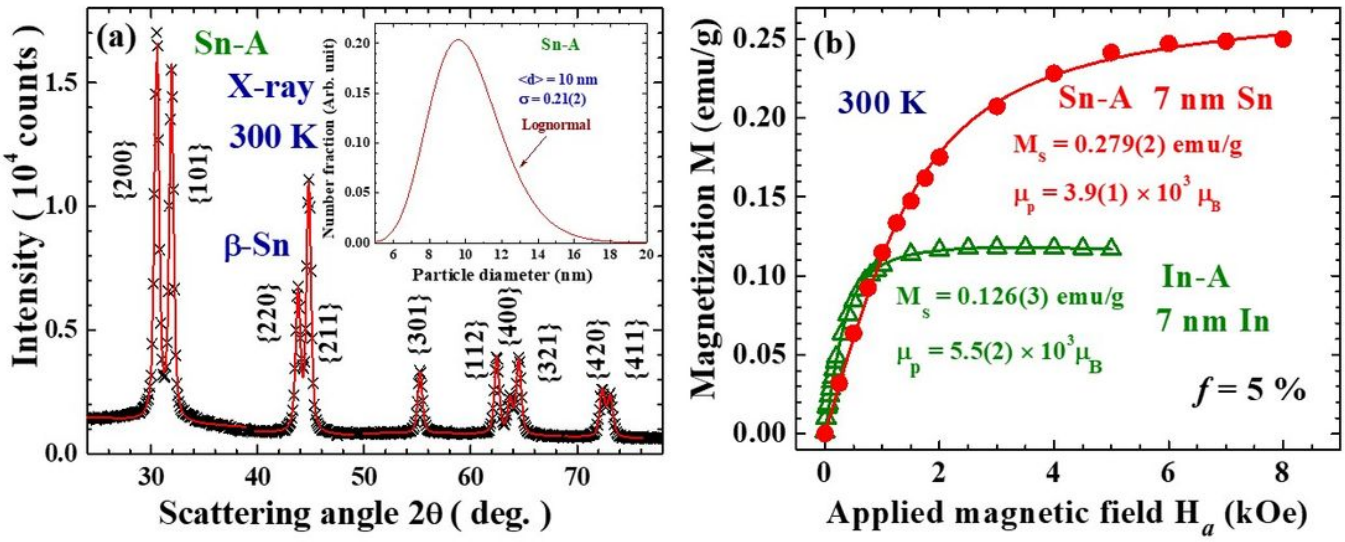

Figure 1

(a) X-ray diffraction pattern of the Sn-A nanoparticle assembly, taken at room temperature, revealing a tetragonal β-Sn structure. The solid curves indicate the calculated profile using the size distribution shown in the inset, giving a mean particle diameter of 10 nm for the Sn-A nanoparticles. (b) Isothermal magnetization curves of 7 nm In-A (open triangles) and 7 nm Sn-A (filled circles) nanoparticle assemblies at a packing fraction of f = 5%, measured in field-increasing loops at 300 K. The solid curves indicate the fits of the data to the Langevin profile, giving saturation magnetizations of 0.126(3) and 0.279(2) emu/g for the 7 nm In-A and 7 nm Sn-A nanoparticles, respectively.

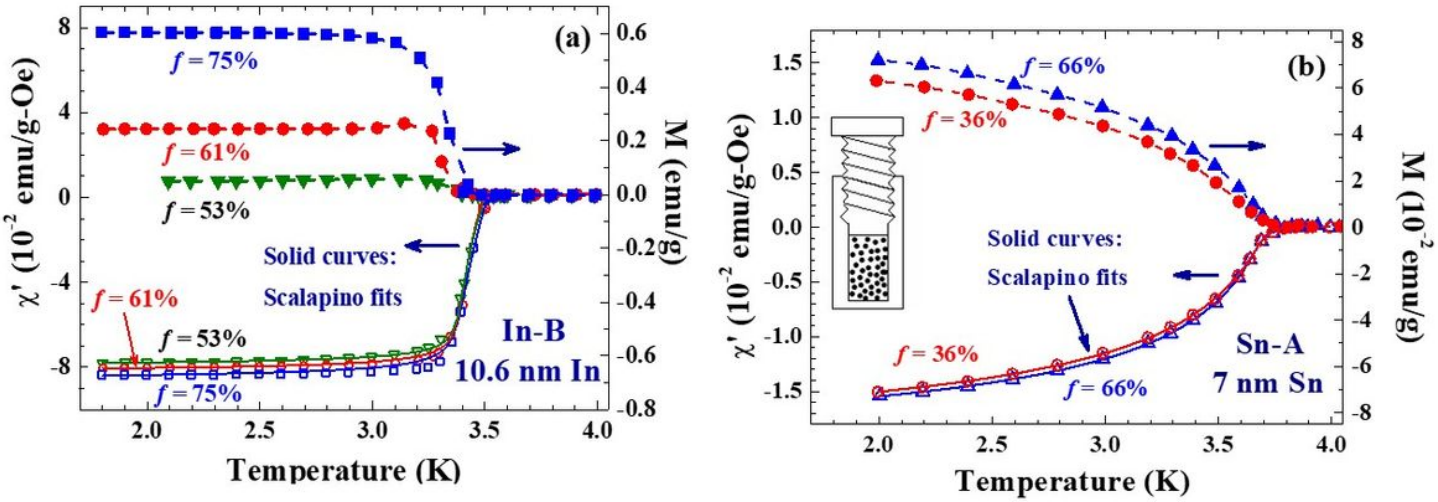

Figure 2

Direct comparison of the M(T) and χ'(T) curves of (a) 10.6 nm In and (b) 7 nm Sn nanoparticle assemblies, taken at various packing fractions. The solid curves on χ'(T) indicate the fits of the data to Scalapino's expression for superconducting screening. The dashed curves on M(T) act as a guide to the eye only. The inset to (b) shows a schematic drawing of the device used to adjust the packing fraction of the nanoparticle assembly.

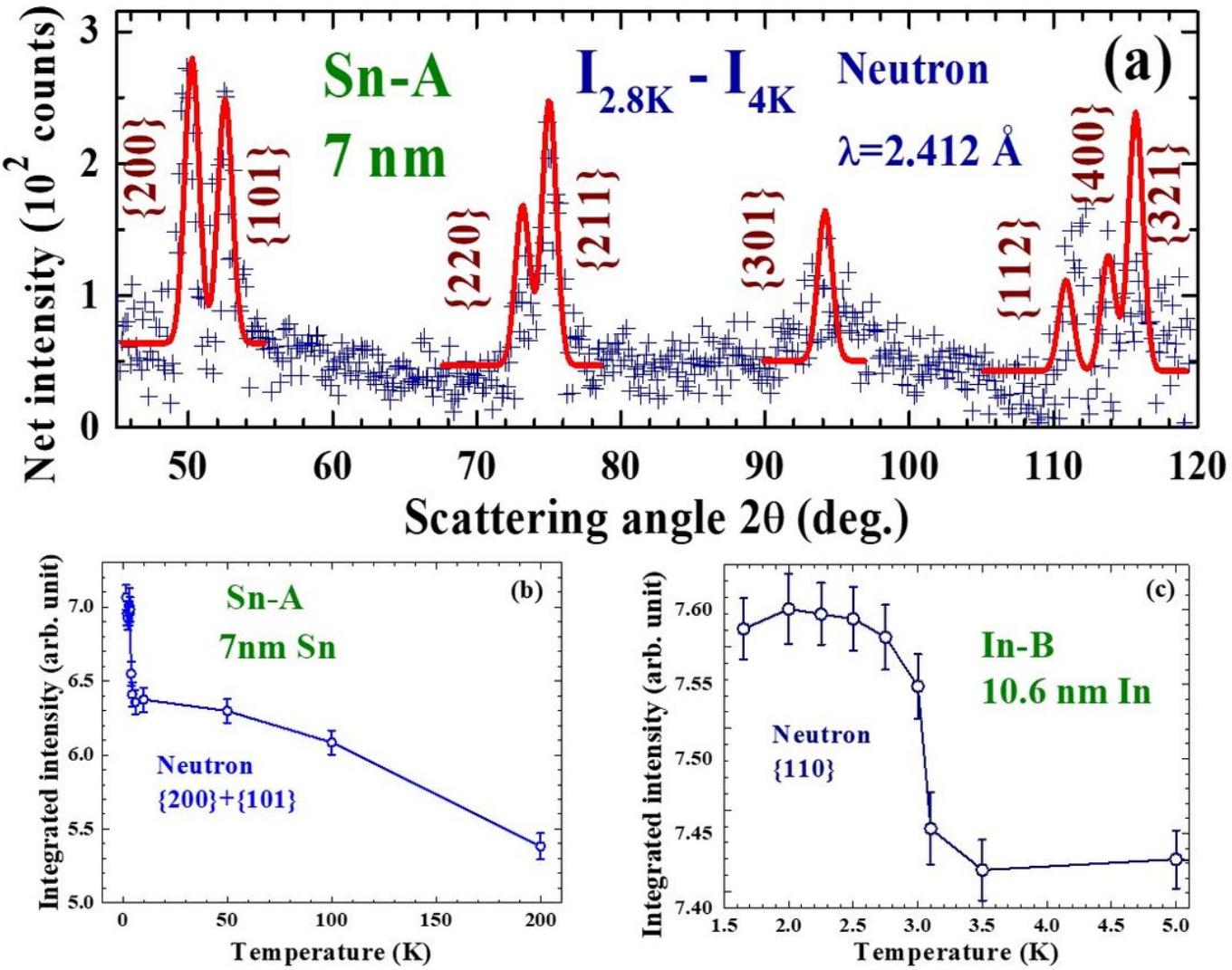

Figure 3

(a) Difference pattern of the 7 nm Sn nanoparticles between the neutron diffraction patterns taken at 2.8 and 4 K, revealing significant enhancement of the reflection intensities in the superconducting state. (b) Temperature dependence of the (200)+(101) reflection of the 7 nm Sn nanoparticles, revealing a ~19% increase in the intensity upon cooling from 200 to 4 K and an additional 10% increase upon further cooling to 1.65 K. (c) Temperature dependence of the (110) reflection of the 10.6 nm In nanoparticles, revealing a progressive increase in the intensity upon cooling to the superconducting state.

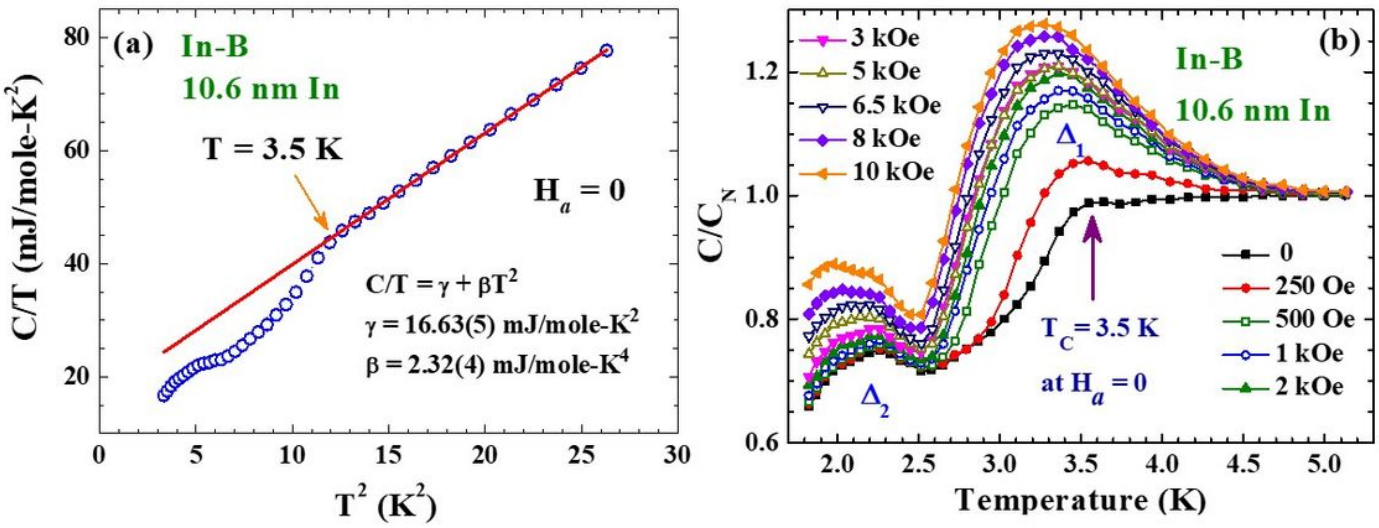

Figure 4

(a) C/T vs T2 plot of the specific heat of the 10.6 nm In nanoparticles. The solid curve shows the results of the fit of the data at high temperatures to the expression listed in the plot. The specific heat departs from the γT+βT3 behavior below 3.5 K. (b) Electronic specific heat of the 10.6 nm In nanoparticles measured under various applied magnetic field, revealing a two-peak structure, labelled Δ1 and Δ2.

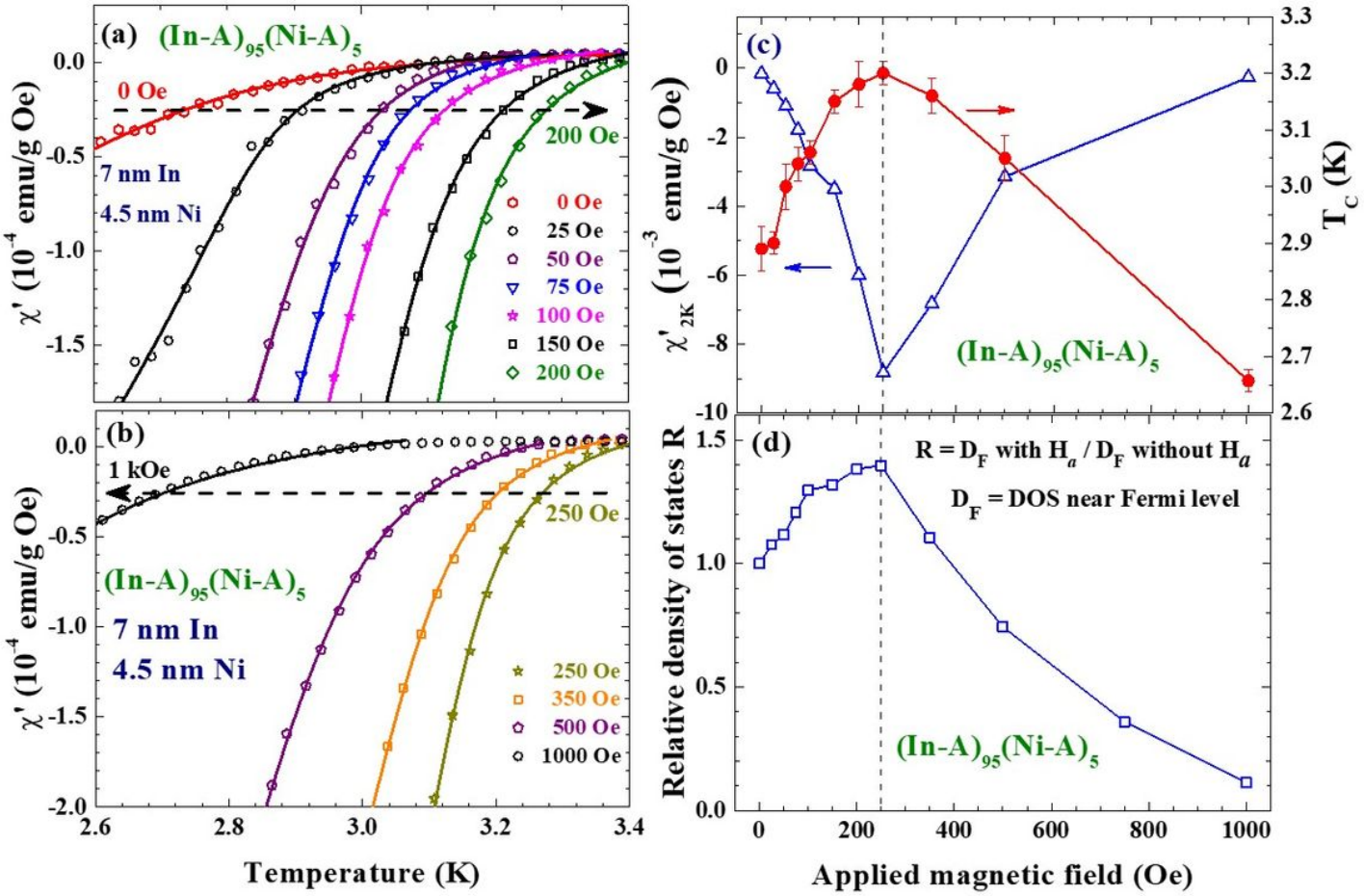

Figure 5

(a)-(b) Effects of the applied magnetic field on the χ'(T) curves of (In-A)95(Ni-A)5 nanoparticle assembly, revealing alterations of TC as the applied magnetic field is changed. The solid curves indicate the results of the fits of the data to Scalapino's expression for superconducting screening. (c) Variations of the value of χ' at 2 K (open triangles) and TC (filled circles) with the applied magnetic field of (In-A)95(Ni-A)5 nanoparticle assembly, revealing a critical magnetic field for maximum TC and diamagnetic response χ'2K. (d) Variation of the relative density of states near the Fermi level R with an applied magnetic field of (In-A)95(Ni-A)5 nanoparticle assembly, revealing a critical magnetic field for maximum R.

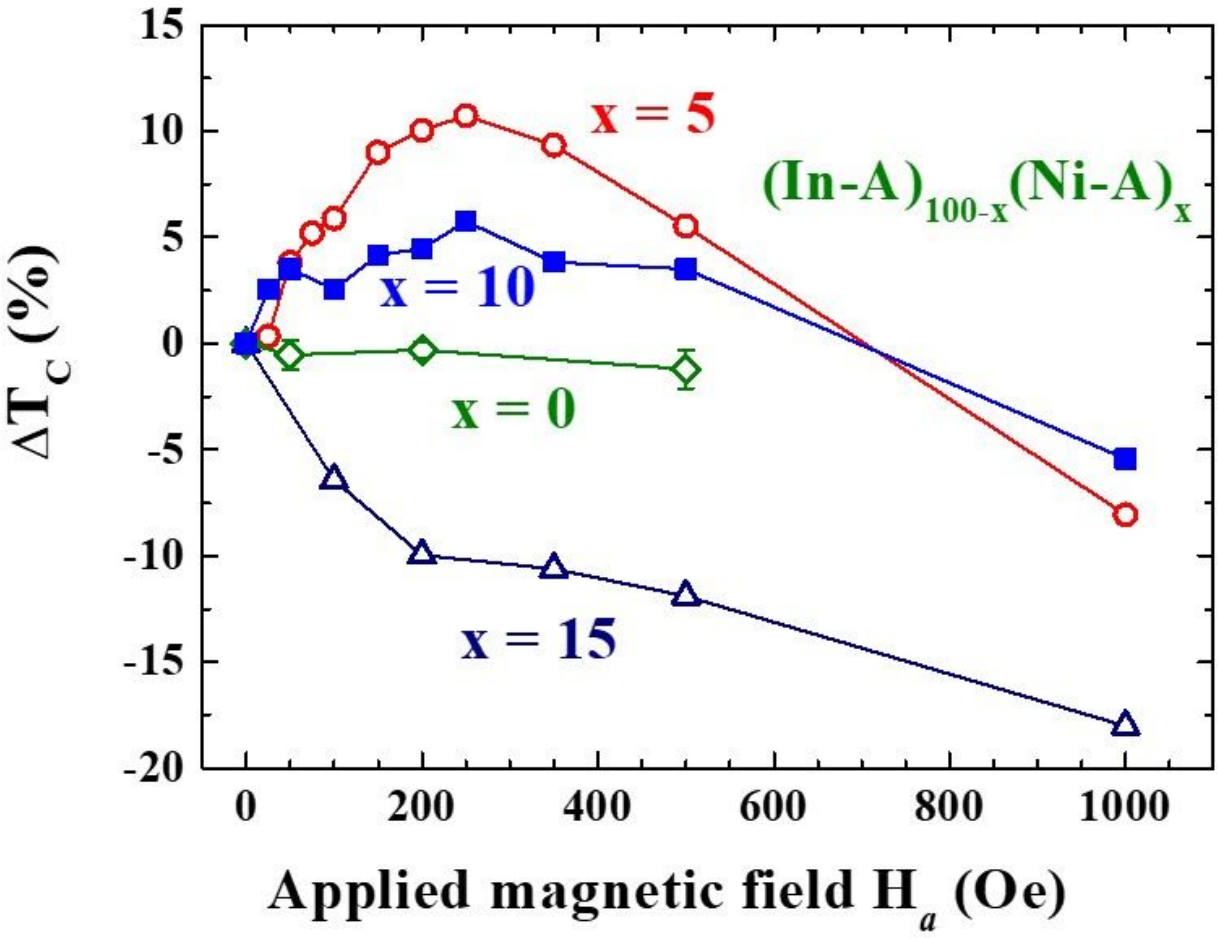

Figure 6

Changes of TC with applied magnetic field of the (In-A)100-x(Ni-A)x nanoparticle assemblies at x = 0 (open diamonds), x =5 (open circles), x =10 (filled squares), and x = 15 (open triangles), revealing the appearance of a critical applied magnetic field for maximum change of TC in the x = 5 and 10 curves.